

## Notice

This is a non-peer reviewed preprint submitted to EarthArXiv. This manuscript has been submitted to Geophysical Research Letters on 02-19-2020 and revised on 06-23-2020 with a reference number 2020GL089490.

Subsequent versions may differ in text and content, please check for the newest version before referencing this preprint.

## Details:

Title: Analytical prediction of seismicity rate due to tides and other oscillating stresses

## Authors:

Elías Rafn Heimisson (Caltech)

Jean-Philippe Avouac (Caltech)

Contact: [eheimiss@caltech.edu](mailto:eheimiss@caltech.edu)

1 **Analytical prediction of seismicity rate due to tides and**  
2 **other oscillating stresses**

3 **Eliás R. Heimisson<sup>1</sup>, and Jean-Philippe Avouac<sup>1</sup>**

4 <sup>1</sup>Division of Geological and Planetary Sciences, California Institute of Technology, Pasadena, CA, USA

5 **Key Points:**

- 6 • We derive a simple analytical model for seismicity rate based on rate-and-state  
7 friction
- 8 • The model can be applied to perpetually oscillating stresses on earth and other  
9 solid-surface bodies
- 10 • We reevaluate recent work on possible tidally triggered seismicity on Mars

**Abstract**

Oscillatory stresses are ubiquitous on earth and other solid-surface bodies. Tides and seasonal signals perpetually stress faults in the crust. Relating seismicity to these stresses offers fundamental insight into earthquake triggering. We present a simple model that describes seismicity rate due to perpetual oscillatory stresses. The model applies to large amplitude, non-harmonic, and quasi-periodic stressing. However, it is not valid for periods larger than the characteristic time  $t_a$ . We show that seismicity rate from short-period stressing scales with the stress amplitude, but for long-periods with the stressing rate. Further, that background seismicity rate  $r$  is equal to the average seismicity rate during short-period stressing. We suggest  $A\sigma_0$  may be underestimated if stresses are approximated by a single harmonic function. We revisit Manga et al. (2019), which analyzed the tidal triggering of Marsquakes, and provide a re-scaling of their seismicity rate response that offers a self-consistent comparison of different hydraulic conditions.

**Plain Language Summary**

The surface of Earth and many other planets and moons is constantly being stressed in an oscillatory manner, for example, by the gravitational pull of moons, planets, and suns. Further, weather, climate, oceans, and other factors may also generate oscillatory stresses. The resulting fluctuations in stress may result in an increased or decreased probability of earthquakes with time. Here we derive a simple formula that can help scientists understand how these oscillatory stresses relate to seismic activity. Moreover, we revisit a recent estimate of the maximum sensitivity of Marsquakes to tides and reach a different conclusion.

**1 Introduction**

Faults in the shallow crust are subject to perpetual, quasi-periodic, oscillatory stress perturbations due to several forcing factors. In particular, oceanic or solid-earth tides, seasonal surface loads due to surface hydrology and the cryosphere, and surface temperature changes. The study of the seismicity response to such stress variations can in principle provide insight into fault friction and earthquake nucleation mechanisms (e.g., Beeler & Lockner, 2003; Scholz et al., 2019; Luo & Liu, 2019; Ader et al., 2014) and possibly inform us of the preparatory phase to impending earthquakes (e.g., Chanard et al., 2019; Tanaka, 2012). Stresses from oscillatory loading are often temporally complex but can

42 be computed with reasonable accuracy (e.g., Lu et al., 2018; Johnson et al., 2020), and  
43 their relationship to changes in seismicity or tremor rate might reveal fundamental in-  
44 sight into earthquake triggering. On Mars and the Moon, such factors might be the dom-  
45 inant source of seismicity (Manga et al., 2019; Duennebier & Sutton, 1974; Lognonne,  
46 2005).

47 Although earthquakes are often weekly correlated to tides, tectonic tremors seem  
48 strongly correlated to tides both in the roots of strike-slip faults (Thomas et al., 2012,  
49 2009) and subduction zones (Rubinstein et al., 2008; Yabe et al., 2015; Houston, 2015).  
50 It has also been observed that slow slip can be modulated by tidal stresses (Hawthorne  
51 & Rubin, 2010). Seasonal variation of seismicity driven by surface load variations have  
52 been reported in several studies (e.g., Bettinelli et al., 2008; Amos et al., 2014; Ueda &  
53 Kato, 2019). However, in most places, the seismicity rate depends weakly on tides (Tanaka  
54 et al., 2002; Cochran et al., 2004), except at mid-ocean ridges, where a particularly strong  
55 response has been observed (e.g., Tolstoy et al., 2002). With the emergence of the next  
56 generation of machine learning and template matching techniques for generating earth-  
57 quake catalogs, which may have ten times the sensitivity of traditional methods (e.g.,  
58 Ross et al., 2019), we will be able to detect and quantify the seismicity response to tidal  
59 and seasonal loading. New developments in observational earthquake seismology, and  
60 the emplacement of a seismometer on Mars, call for a simple model for seismicity rate  
61 under tidal loading that can be compared to data. Here we provide such a model (equa-  
62 tion 8) that can be readily used and has, in practice, only one free parameter in most  
63 applications. Further, we highlight important assumptions, such as ignoring finite fault  
64 effects and discuss potential pitfalls in applying rate-and-state seismicity production mod-  
65 els to oscillatory stresses.

66 Theoretical studies have used the rate-and-state seismicity production model of Dieterich  
67 (1994) to develop an approximate theory for oscillatory stresses. Dieterich (2007) rec-  
68 ognized that for small amplitude and short duration stress changes, the tidally induced  
69 signal could be approximated as the instantaneous response predicted by the Dieterich  
70 (1994) theory. Under these assumptions, Dieterich (2007) derived a simple relationship  
71 for a harmonic stress perturbation. Ader et al. (2014) provided a more general analyt-  
72 ical expression and showed that once some of the assumptions made by Dieterich (2007)  
73 no longer hold, the response is not merely the instantaneous response; however, the anal-  
74 ysis of Ader et al. (2014) was also restricted to a single harmonic perturbation. Because

75 rate-and-state friction is highly non-linear, knowing the response to harmonic pertur-  
76 bations is not sufficient to describe the response to oscillatory stress variations in gen-  
77 eral. For example, tidal loading cannot be explained by a single harmonic perturbation  
78 (e.g., Figure 1), and the formalism of Dieterich (2007) and Ader et al. (2014) would not  
79 allow estimating the expected seismicity response. We, therefore, present a simple ap-  
80 proximate relationship for seismicity rate due to arbitrary long-term oscillatory stress-  
81 ing that is superimposed on the long-term constant stressing rate. The oscillatory stress-  
82 ing can be non-harmonic, quasi-periodic, and include random variations. The approx-  
83 imation is valid as long as the average of the oscillatory stress converges to a mean value  
84 on a time-scale shorter than a characteristic time  $t_a$ . We give a mathematical condition  
85 for when the approximation is valid and provide corrections and alternative expressions  
86 for end-member cases where the approximation breaks down. As an illustration, we re-  
87 visit the analysis of the seismicity response to tidal forcing on Mars of Manga et al. (2019),  
88 based on the solution of Dieterich (1994).

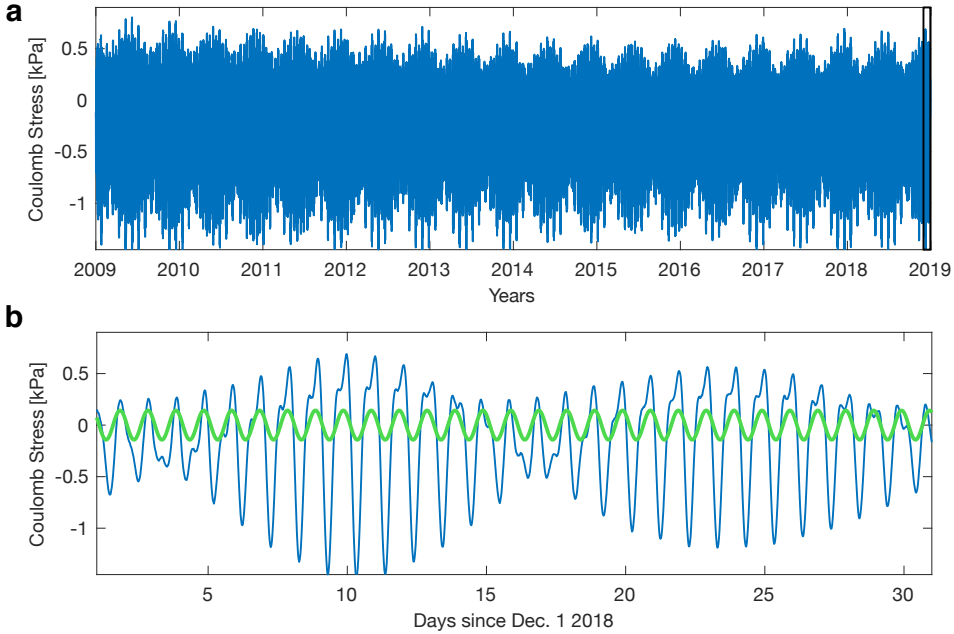


**Figure 1.** Time-series of Coulomb stress changes due to the solid earth tides. **a** 10 years of Coulomb stress perturbations due to solid earth tides on a shallow right-lateral strike-slip fault striking NW-SE and located at Caltech campus. **b** The stress changes in the black box in **a** in blue, green represents the dominant single harmonic mode of the Coulomb stress time series. In section 3.1 we will compute the theoretical seismicity rate during the period in **b** where the entire time-series in **a** is used to fade out the instantaneous initial response.

## 2 Theory

In this section, we present a simple model for triggering due to oscillatory stresses. We refer the reader to Appendix A for the details of the derivation.

Heimisson and Segall (2018) re-derived the Dieterich (1994) theory and showed:

$$R(t) = r \frac{K(t)}{1 + \frac{1}{t_a} \int_0^t K(t') dt'}, \quad (1)$$

where  $R(t)$  is the seismicity rate produced by a population of seismic sources with background seismicity rate  $r$ . The population of seismic sources is assumed to be non-interacting; however, Heimisson (2019) showed that an interacting population could be modeled as an equivalent non-interacting population. This means that we don't expect interaction on average to fundamentally change the response of the system to perturbations. Further,  $t_a = A\sigma_0/\dot{s}_0$  is a characteristic time over which fluctuations in seismicity rate re-

99 turn to the background seismicity, where  $A$  is a constitutive parameter that character-  
 100 izes the rate dependence of friction at steady state, and  $\dot{s}_0 = \dot{\tau}_r - \mu\dot{\sigma}_r$  where  $\mu = \tau_0/\sigma_0 -$   
 101  $\alpha$  is a modified Coulomb background stressing rate that gives rise a steady background  
 102 rate  $r$  in the absence of stress perturbations. Further,  $\tau_0$  and  $\sigma_0$  are the initial background  
 103 shear and effective normal stress respectively acting on a population of seismic sources  
 104 and  $\alpha$  is the Linker-Dieterich constant (Linker & Dieterich, 1992), typically between 0  
 105  $- 0.25$  and describes the instantaneous coupling of normal stress and state. It is worth  
 106 emphasizing that  $\mu$  does thus not represent a coefficient of friction in the traditional sense;  
 107 hence the name modified Coulomb stress.

108 Heimisson and Segall (2018) showed that if changes in normal stress  $\sigma(t)$  are small  
 109 compared to the initial normal stress  $\sigma_0$  then  $K$  is well approximated as:

$$K(t) \approx \exp\left(\frac{S(t)}{A\sigma_0}\right), \quad (2)$$

110 see equation 30 in Heimisson and Segall (2018) for detailed conditions for the validity  
 111 of the approximation. Here  $S(t) = \tau(t) - \mu\sigma(t)$  is the (modified) Coulomb stressing  
 112 history.

113 The presence of the integral in equation 1 and the fact that  $K(t) > 0$  causes per-  
 114 turbations introduced at  $t = 0$  to decay. The short time limit of equation 1 when the  
 115 integral is much smaller than 1 is the instantaneous response due to a perturbation in  
 116 stress:

$$R = rK(t) \approx r \exp\left(\frac{S(t)}{A\sigma_0}\right). \quad (3)$$

117 Dieterich (2007) argued that the instantaneous response (equation 3) is appropriate for  
 118 periodic loading when the period  $T$  is small compared to a characteristic time, which de-  
 119 scribes when the seismicity rate starts decaying, in other words, the onset of the "Omori"  
 120 ( $\sim 1/t$ ) decay following a step change in stress. In Appendix A, we investigate the va-  
 121 lidity of that argument by Dieterich (2007), which has often been applied the tidal trig-  
 122 gering of seismicity and tremor (e.g., Dieterich, 2007; Thomas et al., 2012; Delorey et  
 123 al., 2017; Scholz et al., 2019). In Appendix A, we show for a time-dependent stressing  
 124 history of the form  $S(t) = S_T(t) + \dot{s}_0 t$ , where  $S_T(t)$  is an oscillatory modified coulomb  
 125 stress with a well defined average value (e.g., tidally induced stress) and  $\dot{s}_0$  is a constant  
 126 background stressing rate, and the long term response in seismicity rate is:

$$\frac{R(t)}{r} = \frac{\exp\left(\frac{S_T(t)}{A\sigma_0}\right)}{M}, \quad (4)$$

127 where  $M$  is the average

$$M = \lim_{T \rightarrow \infty} \frac{1}{T} \int_0^T \exp\left(\frac{S_T(t)}{A\sigma_0}\right) dt. \quad (5)$$

128 We note that  $M = 1$  only if  $S_T(t) = 0$ . The average of  $S_T(t)$  may be zero, but  
 129 with non-zero amplitude, we always have  $M > 1$ . Equation 4 generalizes the special  
 130 cases for a harmonic perturbation that was explored by Ader et al. (2014). One impor-  
 131 tant consequence of equations 4 and 5 is that the average seismicity rate  $\bar{R}(t)$  under os-  
 132 cillatory stresses is the same as the background rate  $r$  when no oscillatory stresses oc-  
 133 cur. This can be shown explicitly:

$$\frac{\bar{R}(t)}{r} = \lim_{T \rightarrow \infty} \frac{1}{T} \int_0^T \frac{R(t)}{r} dt = \frac{1}{M} \lim_{T \rightarrow \infty} \frac{1}{T} \int_0^T \exp\left(\frac{S_T(t)}{A\sigma_0}\right) dt = 1. \quad (6)$$

134 In other words, in the presence of general oscillatory stresses, the background rate, in  
 135 the traditional sense expressed by Dieterich (1994), is observable as the average seismic-  
 136 ity rate. This finding is consistent with equation 55 derived by Helmstetter and Shaw  
 137 (2009), which shows that earthquake number is linearly proportional to the stress change  
 138 at  $t \gg t_a$  and thus a zero mean stress change would not induce any change in a num-  
 139 ber of events, for an observation time much longer than  $t_a$ . However, equation 6 is more  
 140 general since it doesn't assume that the mean stress is zero.

141 Let's define  $t_0$  as a zero-crossing time of the oscillatory stress perturbation, i.e.,  $S_T(t_0) =$   
 142 0. Then the rate is

$$R_0 = \frac{r}{M}. \quad (7)$$

143 It can thus be useful to rewrite equation 4

$$R(t) = R_0 \exp\left(\frac{S_T(t)}{A\sigma_0}\right). \quad (8)$$

144 Rate  $R$  is equal to the background average rate  $r$  when there are no oscillatory stresses  
 145 (that is  $R_0 = r$  if  $M = 1$ ), thus the approximation proposed by Dieterich (2007) (equa-  
 146 tion 3) is valid when the stress perturbation is very small compared to  $A\sigma_0$  ( $S_T(t)/A\sigma_0 \ll$

147 1); otherwise, it remains valid within a scaling factor  $M$ . If  $M > 1$  the peak-to-peak  
 148 variation of the seismicity can be significantly overestimated. For many applications, the  
 149 assumption  $S_T(t)/A\sigma_0 \ll 1$  is valid. In applications to aftershocks  $A\sigma_0 \sim 0.01 - 0.1$   
 150 MPa (Hainzl, Steacy, & Marsan, 2010), which is much smaller than tidal stresses ( $\sim 10^{-3} - 10^{-4}$   
 151 MPa, e.g., Figure 1). However, tidal triggering of tectonic tremors near Parkfield has sug-  
 152 gested an average value of  $A\sigma_0 = 6 \cdot 10^{-4}$  MPa (Thomas et al., 2012), in which case  
 153  $S_T(t)/A\sigma_0$  could be on the order of  $0.2 - 2$ . So the  $S_T(t)/A\sigma_0 \ll 1$  assumption is clearly  
 154 violated. Furthermore,  $A\sigma_0$  may be generally different on other planetary bodies com-  
 155 pared to earth (Manga et al., 2019).

156 It is useful to summarize the fundamental underlying assumptions that give rise  
 157 to equation 4 or 8:

- 158 1. The average in equation 5 should converge on a time-scale much less  $t_a$ .
- 159 2. Oscillatory stresses  $S_T(t)$  have been ongoing for a time much larger than  $t_a$ .
- 160 3. Normal stress changes should be modest compared to initial normal stress for the  
 161 Coulomb stress approximation to be valid (Heimisson & Segall, 2018).
- 162 4. Other assumptions of the Dieterich (1994) theory, most importantly, source finite-  
 163 ness can be neglected (see Kaneko & Lapusta, 2008), the population of seismic sources  
 164 is well above steady-state (see Heimisson & Segall, 2018), and neglecting effects  
 165 that arise from source interactions (see Heimisson, 2019).

166 Additional discussion of these assumptions is provided in Appendix A and Appendix  
 167 B, but it is worth highlighting here a fundamental difference that arises when the pe-  
 168 riod of oscillations is much larger than  $t_a$ , and assumption 1 is strongly violated, in which  
 169 case the seismicity rate is proportional to the stressing rate, not the stress:

$$\frac{R(t)}{r} \approx \frac{1}{1 - t_a \frac{\dot{S}_T(t)}{A\sigma_0}}. \quad (9)$$

170 See Appendix B for further discussion.

### 171 3 Examples of applications and comparison with theory

#### 172 3.1 Application to solid-earth tides

173 To test equation 4 against the full solution (equation 1) we generate a time series  
174 of Coulomb stress change using the *Solid* software (Milbert, 2018) representing the (mod-  
175 ified) Coulomb stress changes, with  $\mu = 0.4$ , due to the solid earth tides on shallow right-  
176 lateral strike-slip fault striking NW-SE and located at Caltech campus in California. The  
177 entire time-series is shown in Figure 1a, but we will restrict our attention to the obser-  
178 vation window shown in Figure 1b. Most of the time series in Figure 1a is used to erase  
179 the initial response or initial conditions in equation 1 and compute  $M$ . In the following  
180 we refer to this procedure simply as erasing the initial response. We choose  $t_a = 0.5$   
181 years. We vary  $A\sigma_0$  as described in Figure 2 choosing values that reflect a typical range  
182 of values in aftershock studies: 0.1 and 0.01 MPa (Hainzl, Steacy, & Marsan, 2010) and  
183 a value inferred in studying tidal triggering of tectonic tremors  $6 \cdot 10^{-4}$  MPa (Thomas  
184 et al., 2012). We find that even for large fluctuations in  $R/r$ , equation 4 is in good agree-  
185 ment with the full solution (Figure 2c).

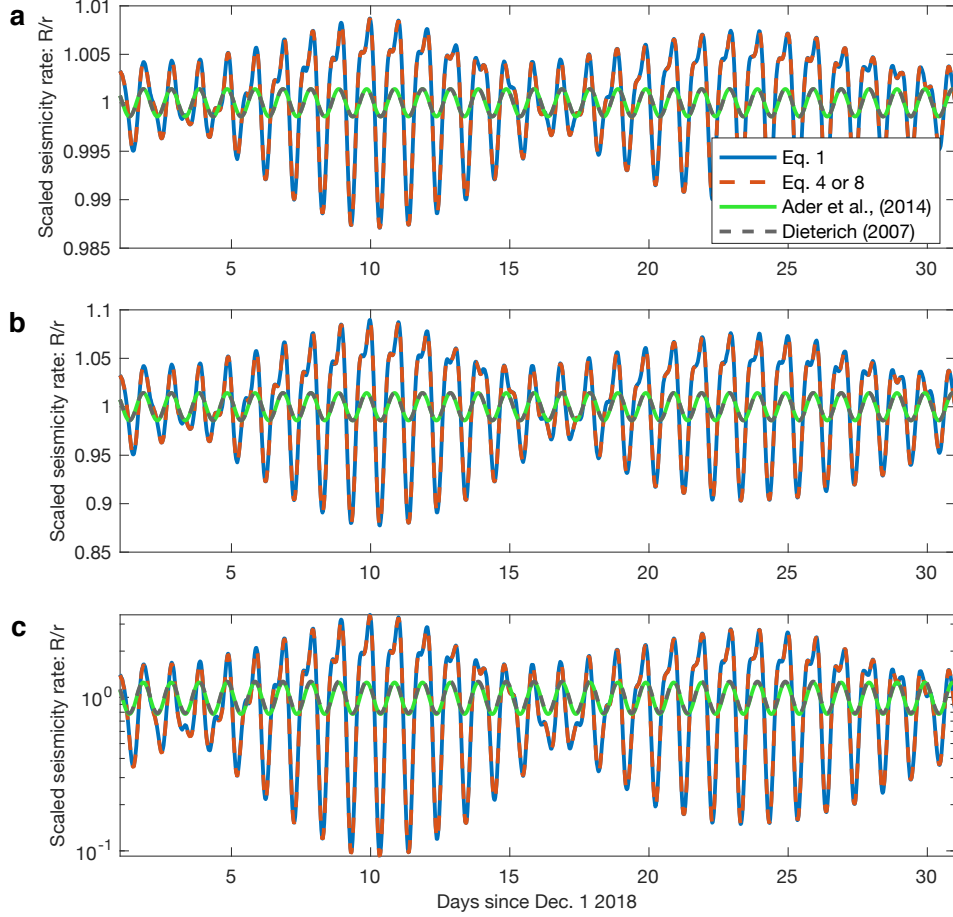


**Figure 2.** Comparison of various approximations and the full solution in equation 1 after the initial response has been faded out. Scaled seismicity rate ( $R/r$ ) for (a)  $A\sigma_0 = 1 \cdot 10^{-1}$  MPa, (b)  $A\sigma_0 = 1 \cdot 10^{-2}$  MPa, (c)  $A\sigma_0 = 6 \cdot 10^{-4}$  MPa (note the logarithmic scale). In all cases equation 4 provides an excellent approximation in all cases with an average relative error of less than 0.002 %, 0.02 %, and 0.7 % in panels a, b, and c respectively. A single harmonic perturbation does not capture the details of the curve shape or amplitude.

186 Corresponding theory for a single harmonic stress perturbation of Dieterich (2007)  
 187 is obtained from equation 3 by representing  $S_T(t)$  by a single harmonic function. Like-  
 188 wise, the harmonic theory of Ader et al. (2014) is obtained in the same manner from equa-  
 189 tion 4. We computed the dominant frequency of the signal in Figure 1a by computing  
 190 a power spectral density. Then find the best fitting amplitude and phase by minimiz-  
 191 ing an  $L_2$  norm that quantifies the residual between the time-series shown in Figure 1a  
 192 and the single harmonic function. The resulting harmonic stress perturbation is shown

193 in Figure 1b in green used to compute the seismicity rate using both the expressions from  
194 Dieterich (2007) and Ader et al. (2014) in Figure 2. The dominant frequency of the earth-  
195 tide signal generally predicts when the seismicity rate is higher or lower than average.  
196 However, the shape and amplitude of the theoretical seismicity rate time-series cannot  
197 be matched with a single harmonic function.

### 198 **3.2 Marsquakes: Reevaluating Manga et al. (2019)**

199 Recently, Manga et al. (2019) argued that Mars might have a clearer relationship  
200 between tides and seismicity rate, which could result in variation as large as two orders  
201 of magnitude in scaled seismicity rate  $R/r$ , also referred to as relative seismicity rate (see  
202 Figure 3 bottom-left panel in Manga et al. (2019)). Their predicted signal was appar-  
203 ently produced based on the initial instantaneous response (Figure 3a) and thus not strictly  
204 correct, as presented. As discussed in the previous section, care needs to be taken to erase  
205 the initial response when applying equation 1 by simulating a time window before the  
206 observation window that is much larger than  $t_a$  and is sufficiently long to estimate  $M$   
207 accurately. If this is not done, the tidal response may be significantly over-estimated, in-  
208 deed by a factor of  $1/M$ .

209 We use equation 1 without erasing the initial response and find a good agreement  
210 with their results (Figure 3a), despite some simplifying assumptions that are detailed  
211 in the next paragraph. Extrapolation of their results suggests that the changes in seis-  
212 micity rate should be much smaller than they estimated (Figure 3b).

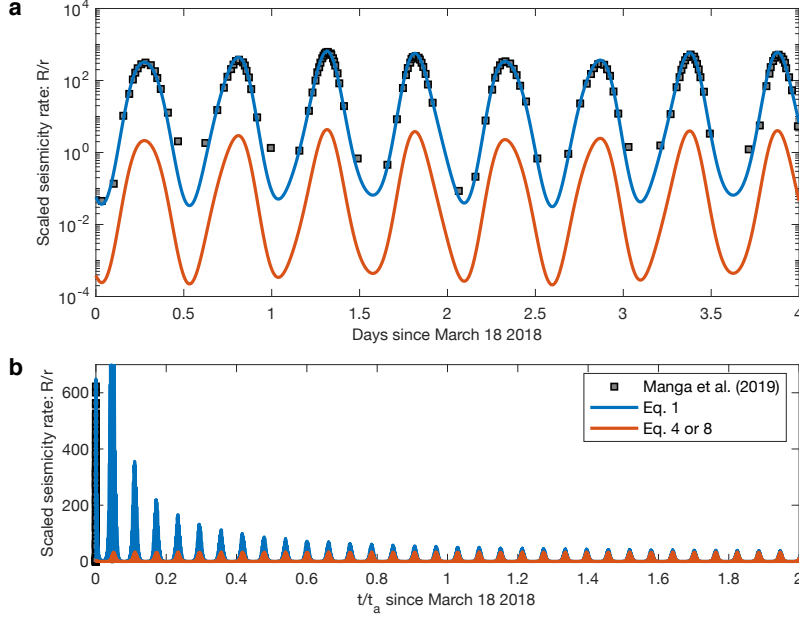


**Figure 3.** Reevaluation of Manga et al. (2019), reveals that they likely overestimated the maximum response by at least a factor of 10. (a) Using an approximate stressing history we observe that equation 1 is in good agreement with the results reported in Figure 3 bottom-left panel in Manga et al. (2019). In contrast, equation 4 suggests that the amplitude should be approximately 100 times less although the shape of the curves is the same. (b) Simulating a time-scale  $t \sim t_a$ , where  $t_a \approx 71.5$  earth years, shows that equation 1 and 4 converge once the initial response gets erased.

213 To replicate the results of Manga et al. (2019), we approximate the Coulomb stress  
 214 perturbations they reported for strike =  $0^\circ$  (Figure 2 in Manga et al. (2019)) by a sum  
 215 of three harmonic functions fitted to a digitized version of their figure. This provides an  
 216 excellent fit to the reported Coulomb stress calculations during the four days window  
 217 they show. However, the long term extrapolation in Figure 3b shows that the seismic-  
 218 ity rate decays over a time-scale of  $t \sim t_a$ , before reaching the expected rate variation  
 219 due to tidal loading that would be observable.

220 Fortunately, the ratio between the instantaneous response and the long-term re-  
 221 sponse is  $M$ . Thus from equation 8 we can conclude that the reported relative rate of  
 222 Manga et al. (2019) is correct if interpreted as relative to  $R_0$ , but not  $r$  as they stated.  
 223 One important consequence is that the difference in seismicity rate shown in different  
 224 panels in Figure 3 in Manga et al. (2019) (showing response due to variations in effec-

225 tive normal stress) does not reflect relative changes in absolute seismicity rate. In their  
 226 top panels  $M \approx 1$ , in the bottom panels  $M \approx 100$ . The maximum rate in the bottom  
 227 panel is  $\approx 600$ , but for the top  $\approx 1$ . Thus, the difference in maximum absolute seismic-  
 228 ity rate, of the two scenarios, is only about a factor of 6.

## 229 4 Discussion

230 Equations 4 or 8 offer an estimate of the seismicity rate produced by a population  
 231 of seismic sources due to a stressing history produced by a constant stressing rate and  
 232 oscillating stress sources. These equations are perfectly equivalent and simple to use, given  
 233 that the stressing history is known, there is only one free parameter that may need to  
 234 be fitted:  $A\sigma_0$ . In case of observations of a seismicity response to a known stressing his-  
 235 tory, they might thus be used to assess the validity of the theory for seismicity rate based  
 236 on rate-and-state friction (Dieterich, 1994; Heimisson & Segall, 2018) and place constraints  
 237 on the friction law. Further, estimating  $A\sigma_0$  by using tides or seasonal stress variations  
 238 has implications for physics-based forecasts of aftershocks, where this parameter also needs  
 239 to be estimated (e.g. Hainzl, Brietzke, & Zoller, 2010). Thus tides could be used in ad-  
 240 vance to or map spatial variations of this parameter. Those values could then be used  
 241 for aftershock forecasts once an earthquake occurs or forecast induced seismicity expected  
 242 in response to anthropogenic stress changes.

243 Equation 8 may be preferred in some data applications compared to equation 4.  
 244 Remarkably, Yabe et al. (2015) and Scholz et al. (2019) successfully applied equation 8  
 245 in good agreement with data without explicit theoretical underpinnings. While Yabe et  
 246 al. (2015) correctly state that  $R_0$  is a reference rate when tidal stress is zero, the latter  
 247 study refers to  $R$  as "the instantaneous seismicity rate". We have shown here that  $R$  in  
 248 equation 3 represents the instantaneous seismicity rate, but equation 8 is the approx-  
 249 imate seismicity rate in the presence of long term response tidal loading or other oscil-  
 250 latory stresses.  $R_0 \neq r$ , unless  $|S_T(t)|/A\sigma_0 \ll 1$  for all  $t$ , in which case  $R_0 \approx r$ .

251 The approximation made in equation 4 or 8 is not valid in the limit of a very long  
 252 period stress variations that are larger than  $t_a$ , as described by equation 9. In this case,  
 253 we expect the seismicity rate to be proportional to the stressing rate, but not the stress.  
 254 Beeler and Lockner (2003) conducted experiments on a saw-cut sample in a triaxial load-  
 255 ing frame. They imposed oscillatory stresses on a constant stressing rate and found that

256 for short periods compared to the nucleation time, changes in event probability was in  
 257 phase with the stress. However, for long periods the probability of events was propor-  
 258 tional to and in phase with the stressing rate. Their finding is in agreement with our the-  
 259 oretical results.

260 Johnson et al. (2017) investigated the relationship between seismicity rate and sea-  
 261 sonal variations in shear stress and stress rate in California. Depending on fault orien-  
 262 tation, they identified a weak correlation of seismicity rate with either shear stressing  
 263 rate or stress. This finding would suggest that, on average,  $t_a$  changes with fault orien-  
 264 tation. That is reasonable since background stressing rates must vary with fault orien-  
 265 tation. We emphasize that when investigating seasonal changes in seismicity rate, which  
 266 may be on a similar time-scale as  $t_a$ , one must be careful in picking the appropriate ap-  
 267 proximation (either 4 or 9). We strongly suggest that equation 1 should be used for ref-  
 268 erence after erasing the initial response. Further, we recall that our analysis assumes that  
 269 a single degree of freedom spring-and-slider system can approximate the response of a  
 270 fault to a stress perturbation. Significant differences have been observed if finite fault  
 271 effects need to be taken into account (e.g. Kaneko & Lapusta, 2008; Ampuero & Rubin,  
 272 2008; Rubin & Ampuero, 2005). Simulations indicate that this happens if the typical pe-  
 273 riod of the stress perturbation is of the order of  $2\pi t_a$  (Ader et al., 2014). In that case,  
 274 the approximate analytical solutions described in this study would not apply.

275 Using a single harmonic function to represent the oscillating stressing history may  
 276 be desirable due to the simplicity of the problem and the fact that spectral analysis, such  
 277 as the Schuster spectra, can be used to extract the dominant period of the seismicity rate  
 278 (Ader et al., 2014). However, this may lead to a bias in the estimate of  $A\sigma_0$  if the stress-  
 279 ing history has multiple components that can add up coherently. Let us assume that the  
 280 stressing history is composed of  $N$  harmonic components:

$$S_T(t) = \sum_{i=1}^N c_i \sin\left(\frac{2\pi t}{T_i} + \phi_i\right) \quad (10)$$

281 where the amplitudes are sorted:  $c_1 > c_2 > \dots > c_N$  and thus  $T_1$  is the dominant pe-  
 282 riod. Using equation 8 and only the dominant harmonic component of the  $S_T(t)$  then  
 283 one finds:

$$\log\left(\frac{\max(R)}{R_0}\right) = \frac{c_1}{(A\sigma_0)_{SH}}, \quad (11)$$

284 where  $(A\sigma_0)_{SH}$  represent the estimate of  $A\sigma_0$  under the assumption of a single harmonic,  
 285 and  $\max(R)$  is the maximum observed seismicity rate. However, for multiple harmon-  
 286 ics we find:

$$\log\left(\frac{\max(R)}{R_0}\right) = \max\left(\frac{\sum_{i=1}^N c_i \sin\left(\frac{2\pi t}{T_i} + \phi_i\right)}{(A\sigma_0)_{MH}}\right) \leq \frac{\sum_{i=1}^N |c_i|}{(A\sigma_0)_{MH}}, \quad (12)$$

287 where  $(A\sigma_0)_{MH}$  represents the estimate of  $A\sigma_0$  under the assumption of multiple har-  
 288 monics. Thus we conclude that the ratio of the two estimates is bounded in the follow-  
 289 ing manner:

$$\frac{(A\sigma_0)_{MH}}{(A\sigma_0)_{SH}} \leq \frac{\sum_{i=1}^N |c_i|}{|c_1|}. \quad (13)$$

290 Therefore, we expect that  $A\sigma_0$  is typically underestimated if a single harmonic stress source  
 291 is assumed. This conclusion is consistent with Figure 2, which shows that the amplitude  
 292 is not well match by a single harmonic. However, dividing  $A\sigma_0$  by factor 5.3 would al-  
 293 low the single harmonic approximation to match the maximum rate of the full solution.  
 294 Equation 13 thus successfully offers an inequality constraint of  $(A\sigma_0)_{MH} \leq 30 \cdot (A\sigma_0)_{SH}$ .

## 295 5 Conclusions

296 We have derived a simple approximate equation to quantify the relationship be-  
 297 tween seismicity and oscillatory stresses, based on assuming an earthquake nucleation  
 298 process governed by rate-and-state friction. This relationship may be used, for exam-  
 299 ple, in theoretical or observational studies of seismicity response to tidal and seasonal  
 300 loading (equation 4 or 8). In applications to observations, only one free parameter ( $A\sigma_0$ )  
 301 needs to be determined. We compare our approximations to using the dominant harmonic  
 302 mode of the stresses and to the full solution (1) where the initial response has been care-  
 303 fully erased. We conclude that in most cases, our approximation is in excellent agree-  
 304 ment with the full solution and is much more accurate than using a single harmonic stress  
 305 perturbation. Our analysis shows that seismicity rate on Mars due to tides calculated  
 306 by Manga et al. (2019) was reported as relative to the seismicity rate at zero stress  $R_0$   
 307 and not the background rate  $r$ . This has implications for how amplitudes of seismicity  
 308 rate fluctuations vary for different hydraulic conditions that alter the effective normal

309 stress. We have here provided a simple equation 4 that may be used to reevaluate this  
 310 effect or, more generally, the seismicity response expected from stress variations on earth  
 311 and solid-surface bodies, provided that fault finite-size effects can be neglected. Finally,  
 312 we have shown in equation 6 that the constant background rate  $r$  postulated by Dieterich  
 313 (1994) due to a constant stressing rate is an observable quantity in the presence of long-  
 314 term oscillatory stresses as the average seismicity rate  $\bar{R}(t)$ .

### 315 Acknowledgments

316 This is a theoretical paper and contains no data. This research was partly supported by  
 317 NSF award EAR-1821853. We thank two anonymous reviewers for their constructive re-  
 318 marks that significantly improved this manuscript.

### 319 Appendix A Derivation of equation 4

320 We write the stressing history as the sum of steady stressing rate ( $\dot{s}_0 t$ ) and time-  
 321 dependent stress perturbation  $S_T(t)$ , i.e.  $S(t) = S_T(t) + \dot{s}_0 t$  and obtain

$$K(t) = \exp\left(\frac{S(t)}{A\sigma_0}\right) = \exp\left(\frac{S_T(t)}{A\sigma_0} + \frac{t}{t_a}\right) = \eta(t) \exp\left(\frac{t}{t_a}\right). \quad (\text{A1})$$

322 We assume  $\eta(t)$  is a function with the following property

$$\eta(t) = M + \epsilon(t), \text{ where } M = \lim_{T \rightarrow \infty} \frac{1}{T} \int_0^T \eta(t) dt \text{ with } |M| < \infty, \quad (\text{A2})$$

323 it follows that

$$\lim_{T \rightarrow \infty} \frac{1}{T} \int_0^T \eta(t) dt = \lim_{T \rightarrow \infty} \frac{1}{T} \int_0^T M dt + \frac{1}{T} \int_0^T \epsilon(t) dt = M + \lim_{T \rightarrow \infty} \frac{1}{T} \int_0^T \epsilon(t) dt. \quad (\text{A3})$$

324 In other words,  $M$  is the average of  $\eta(t)$  and  $|M| < \infty$ ; thus the average of  $\epsilon(t)$  is zero,  
 325 that is

$$\lim_{T \rightarrow \infty} \frac{1}{T} \int_0^T \epsilon(t) dt = 0. \quad (\text{A4})$$

326 For example, any periodic bounded function  $\eta(t) = \eta(t+T)$ , satisfies these conditions.

327 In this case, the physical interpretation of  $\eta(t)$  is  $\log(\eta(t)) = S_p(t)/A\sigma_0$  where  $S_p(t) =$   
 328  $S_p(t+T)$  is a periodic stress perturbation. There is no requirement that  $S_p(t)$  be a har-  
 329 monic perturbation, such as previously explored (Ader et al., 2014; Dieterich, 2007). If

330  $\eta(t)$  is periodic then equation A1 describes a combination of steady stressing rate ( $t_a =$   
 331  $A\sigma_0/\dot{\tau}_0$ ) and a sum of periodic stress perturbations that represent the oscillatory load-  
 332 ing. However, tidal loading has multiple harmonic components and their periods do not  
 333 exactly differ by an integer. The resulting stressing history is not periodic. However, we  
 334 can still write  $\eta(t) = \exp(S_T(t)/A\sigma_0) = M + \epsilon(t)$ . Further, we could imagine that  $\epsilon(t)$   
 335 contains a stochastic component with a well defined mean. We shall now derive the long  
 336 term behavior of a population of seismic sources that is persistently subject to a stress-  
 337 ing history that can be written in the form of equation A1.

338 Once the integral in the denominator of equation 1 is much larger than 1 we may  
 339 simplify

$$\frac{R(t)}{r} = \frac{K(t)}{\frac{1}{t_a} \int_0^t K(t') dt'}, \quad (\text{A5})$$

340 or using the notation in equation A1

$$\frac{R(t)}{r} = \frac{\eta(t) \exp\left(\frac{t}{t_a}\right)}{\frac{1}{t_a} \int_0^t \eta(t') \exp\left(\frac{t'}{t_a}\right) dt'}. \quad (\text{A6})$$

341 Substitution with A2 yields

$$\int_0^t \eta(t') \exp\left(\frac{t'}{t_a}\right) dt' = t_a M \exp\left(\frac{t}{t_a}\right) + \int_0^t \epsilon(t') \exp\left(\frac{t'}{t_a}\right) dt' \quad (\text{A7})$$

342 and we get:

$$\frac{R(t)}{r} = \frac{\eta(t)}{M + \frac{1}{t_a} \int_0^t \epsilon(t') \exp\left(\frac{-(t-t')}{t_a}\right) dt'}. \quad (\text{A8})$$

343 We recognize that  $\int_0^t \epsilon(t') \exp\left(\frac{-(t-t')}{t_a}\right) dt'$  is simply a convolution. The function  $\exp(-(t-t')/t_a)$ ,  
 344 imposes a memory effect and essentially eliminates any contribution in fluctuations in  
 345  $\epsilon(t)$  in a time window of that lies significantly outside times  $t-t_a$  to  $t$ . Thus if  $\epsilon(t)$  av-  
 346 erages to 0 on a time-scale that is significantly shorter than  $t_a$  the integral can gener-  
 347 ally be ignored. For example, this condition is satisfied if the oscillatory stresses and pos-  
 348 sible random stresses, average to approximately zero on a time-scale smaller than  $t_a$ . More  
 349 precisely, the integral can be ignored if the following condition applies:

$$\left| \frac{\frac{1}{t_a} \int_0^t \epsilon(t') \exp\left(\frac{-(t-t')}{t_a}\right) dt'}{M} \right| \ll 1, \text{ for all } t, \quad (\text{A9})$$

350 then equation A8 reduces to

$$\frac{R(t)}{r} = \frac{\eta(t)}{M} = \frac{\exp\left(\frac{S_T(t)}{A\sigma_0}\right)}{M}. \quad (\text{A10})$$

## 351 Appendix B Validity of equations 4/8

352 Here we offer further analysis on the validity of equation 4 or 8 and provide some  
 353 insight into the regimes when they are not valid. The validity of equation 4 or 8 rests  
 354 on the validity of equation A9. We investigate two different expansions of the relevant  
 355 term through repeated integration by parts:

$$\frac{1}{t_a} \exp\left(-\frac{t}{t_a}\right) \int \epsilon(t') \exp\left(\frac{t'}{t_a}\right) dt' = \frac{\epsilon^{-1}(t)}{t_a} - \frac{\epsilon^{-2}(t)}{t_a^2} + \frac{\epsilon^{-3}(t)}{t_a^3} + \dots \quad (\text{B1})$$

$$\frac{1}{t_a} \exp\left(-\frac{t}{t_a}\right) \int \epsilon(t') \exp\left(\frac{t'}{t_a}\right) dt' = \epsilon - t_a \epsilon^1(t) + t_a^2 \epsilon^2(t) - t_a^3 \epsilon^3(t) + \dots \quad (\text{B2})$$

356 where  $\epsilon^n$  is the  $n$ -th derivative of  $\epsilon$  and  $\epsilon^{-n}$  is the  $n$ -th indefinite integral (or anti-derivative)  
 357 of  $\epsilon$ . If the largest period,  $T_{max}$  in the Fourier decomposition of  $\epsilon$  with a non-zero co-  
 358 efficient satisfies  $T_{max} < t_a$  then the  $n$ -th term in equation B1 will be a correction of  
 359 order  $O(T_{max}^n/t_a^n)$ , and convergence is expected. For long period changes  $T_{min} > t_a$ ,  
 360 equation B2 provides an expansion where we have  $O(t_a^n/T_{min}^n)$  correction for the  $n$ -th  
 361 term.

362 In the short period limit,  $T_{max} < t_a$ , we find a first-order correction to equation  
 363 4:

$$\frac{R(t)}{r} = \frac{\exp\left(\frac{S_T(t)}{A\sigma_0}\right)}{M + \frac{\epsilon^{-1}(t)}{t_a}}, \quad (\text{B3})$$

364 where in practice we compute  $\epsilon^{-1}(t)$  using the following equation unless the indefinite  
 365 integral is known analytically.

$$\epsilon^{-1}(t) = \int_{-t_0}^t \exp\left(\frac{S_T(t)}{A\sigma_0}\right) dt - Mt, \quad (\text{B4})$$

366 where  $t_0 > 0$  is chosen sufficiently large to erase the influence of the initial stress value  
 367 in the integral. Numerical exploration of equation B3 suggested that the additional cor-  
 368 rection term is typically small and unlikely to be useful in practical applications.

369 In the long period limit,  $T_{min} > t_a$ , we get,

$$\frac{R(t)}{r} = \frac{\exp\left(\frac{S_T(t)}{A\sigma_0}\right)}{\exp\left(\frac{S_T(t)}{A\sigma_0}\right) - t_a \exp\left(\frac{S_T(t)}{A\sigma_0}\right) \frac{\dot{S}_T(t)}{A\sigma_0}} = \frac{1}{1 - t_a \frac{\dot{S}_T(t)}{A\sigma_0}} \approx 1 + t_a \frac{\dot{S}_T(t)}{A\sigma_0}, \quad (\text{B5})$$

370 where the approximation represents a first order Taylor expansion. Equation B5 may  
 371 be useful when investigating long term behavior such as seasonal changes if  $t_a$  is shorter  
 372 than 1 year as is probably the case in active tectonic settings (e.g. Bettinelli et al., 2008).  
 373 Notably, equation 9 depends on the stressing rate, not directly the stress, and is to the  
 374 first order linearly proportional to the stressing rate (Figure B1). Implying that, in this  
 375 particular limit, the seismicity rate is out of phase with the stress variations. This re-  
 376 sult is consistent with the findings of Helmstetter and Shaw (2009) for slowly varying  
 377 stresses and the experimental results of Beeler and Lockner (2003) (see Discussion for  
 378 more details). Furthermore, we see that equation 4 is not valid in this limit since it pre-  
 379 dictes that the seismicity rate is proportional to the stress change, not the stressing rate.

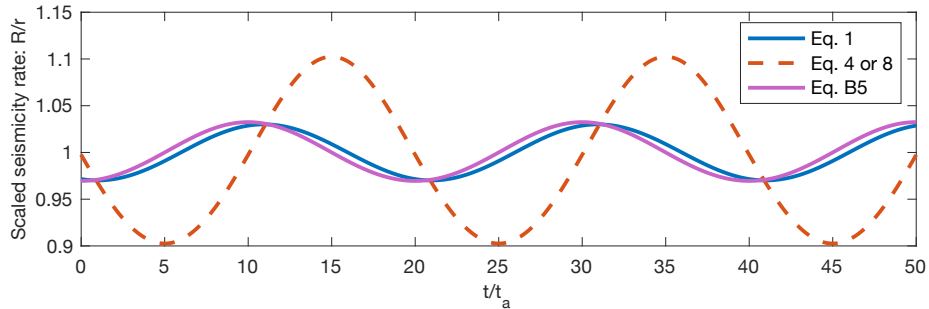


**Figure B1.** Simulations of seismicity rate response for  $S_T(t)/A\sigma_0 = -0.1 \cdot \sin(2\pi t/T) + t/t_a$ , where the period  $T = 20t_a$ . In this limit equation 9 predicts that the seismicity rate should be in phase the stressing rate and the equations 4 or 8 are in no agreement with the full solution 1

## 380 References

381 Ader, T. J., Lapusta, N., Avouac, J.-P., & Ampuero, J.-P. (2014, 05). Response of  
 382 rate-and-state seismogenic faults to harmonic shear-stress perturbations. *Geo-*

- 383 *physical Journal International*, 198(1), 385-413. doi: 10.1093/gji/ggu144
- 384 Amos, C. B., Audet, P., Hammond, W. C., Bürgmann, R., Johanson, I. A., & Ble-  
 385 witt, G. (2014). Uplift and seismicity driven by groundwater depletion in  
 386 central california. *Nature*, 509(7501), 483-486. doi: 10.1038/nature13275
- 387 Ampuero, J.-P., & Rubin, A. M. (2008). Earthquake nucleation on rate and state  
 388 faults – aging and slip laws. *Journal of Geophysical Research: Solid Earth*,  
 389 113(B1). doi: 10.1029/2007JB005082
- 390 Beeler, N. M., & Lockner, D. A. (2003). Why earthquakes correlate weakly with the  
 391 solid earth tides: Effects of periodic stress on the rate and probability of earth-  
 392 quake occurrence. *Journal of Geophysical Research: Solid Earth*, 108(B8). doi:  
 393 10.1029/2001JB001518
- 394 Bettinelli, P., Avouac, J.-P., Flouzat, M., Bollinger, L., Ramillien, G., Rajaure, S., &  
 395 Sapkota, S. (2008). Seasonal variations of seismicity and geodetic strain in the  
 396 himalaya induced by surface hydrology. *Earth and Planetary Science Letters*,  
 397 266(3), 332-344. doi: 10.1016/j.epsl.2007.11.021
- 398 Chanard, K., Nicolas, A., Hatano, T., Petrelis, F., Latour, S., Vinciguerra, S., &  
 399 Schubnel, A. (2019). Sensitivity of acoustic emission triggering to small pore  
 400 pressure cycling perturbations during brittle creep. *Geophysical Research*  
 401 *Letters*, 46(13), 7414-7423. doi: 10.1029/2019GL082093
- 402 Cochran, E. S., Vidale, J. E., & Tanaka, S. (2004). Earth tides can trigger shallow  
 403 thrust fault earthquakes. *Science*, 306(5699), 1164-1166. doi: 10.1126/science  
 404 .1103961
- 405 Delorey, A. A., van der Elst, N. J., & Johnson, P. A. (2017). Tidal triggering of  
 406 earthquakes suggests poroelastic behavior on the san andreas fault. *Earth and*  
 407 *Planetary Science Letters*, 460, 164 - 170. doi: [https://doi.org/10.1016/j.epsl](https://doi.org/10.1016/j.epsl.2016.12.014)  
 408 [.2016.12.014](https://doi.org/10.1016/j.epsl.2016.12.014)
- 409 Dieterich, J. (1994). A constitutive law for rate of earthquake production and its  
 410 application to earthquake clustering. *J. Geophys. Res. Solid Earth*, 99(B2),  
 411 2601-2618. doi: 10.1029/93JB02581
- 412 Dieterich, J. (2007). 4.04 - applications of rate- and state-dependent friction to  
 413 models of fault-slip and earthquake occurrence. In G. Schubert (Ed.), *Treatise*  
 414 *on geophysics (second edition)* (Second Edition ed., p. 93 - 110). Oxford: El-  
 415 sevier. Retrieved from <http://www.sciencedirect.com/science/article/>

- 416 pii/B9780444538024000750 doi: <https://doi.org/10.1016/B978-0-444-53802-4>  
 417 .00075-0
- 418 Duennebier, F., & Sutton, G. H. (1974). Thermal moonquakes. *Journal of Geophys-*  
 419 *ical Research (1896-1977)*, 79(29), 4351-4363. doi: 10.1029/JB079i029p04351
- 420 Hainzl, S., Brietzke, G. B., & Zoller, G. (2010). Quantitative earthquake forecasts  
 421 resulting from static stress triggering. *Journal of Geophysical Research: Solid*  
 422 *Earth*, 115(B11). doi: 10.1029/2010JB007473
- 423 Hainzl, S., Steacy, S., & Marsan, D. (2010). Seismicity models based on coulomb  
 424 stress calculations. *CORSSA: Community Online Resource for Statis-*  
 425 *tical Seismicity Analysis*. Retrieved from [https://doi.org/10.5078/](https://doi.org/10.5078/corssa-32035809)  
 426 [corssa-32035809](https://doi.org/10.5078/corssa-32035809)
- 427 Hawthorne, J. C., & Rubin, A. M. (2010). Tidal modulation of slow slip in casca-  
 428 dia. *Journal of Geophysical Research: Solid Earth*, 115(B9). doi: 10.1029/  
 429 2010JB007502
- 430 Heimisson, E. R. (2019). Constitutive law for earthquake production based  
 431 on rate-and-state friction: Theory and application of interacting sources.  
 432 *Journal of Geophysical Research: Solid Earth*, 124(2), 1802-1821. doi:  
 433 10.1029/2018JB016823
- 434 Heimisson, E. R., & Segall, P. (2018). Constitutive law for earthquake production  
 435 based on rate-and-state friction: Dieterich 1994 revisited. *Journal of Geophysi-*  
 436 *cal Research: Solid Earth*, 123(5), 4141-4156. doi: 10.1029/2018JB015656
- 437 Helmstetter, A., & Shaw, B. E. (2009). Afterslip and aftershocks in the rate-and-  
 438 state friction law. *Journal of Geophysical Research: Solid Earth*, 114(B1). doi:  
 439 10.1029/2007JB005077
- 440 Houston, H. (2015). Low friction and fault weakening revealed by rising sensitiv-  
 441 ity of tremor to tidal stress. *Nature Geoscience*, 8(5), 409-415. doi: 10.1038/  
 442 ngeo2419
- 443 Johnson, C. W., Fu, Y., & Bürgmann, R. (2017). Seasonal water storage, stress  
 444 modulation, and california seismicity. *Science*, 356(6343), 1161-1164. doi: 10  
 445 .1126/science.aak9547
- 446 Johnson, C. W., Fu, Y., & Bürgmann, R. (2020). Hydrospheric modulation of stress  
 447 and seismicity on shallow faults in southern alaska. *Earth and Planetary Sci-*  
 448 *ence Letters*, 530, 115904. doi: 10.1016/j.epsl.2019.115904

- 449 Kaneko, Y., & Lapusta, N. (2008). Variability of earthquake nucleation in  
 450 continuum models of rate-and-state faults and implications for aftershock  
 451 rates. *Journal of Geophysical Research: Solid Earth*, *113*(B12). doi:  
 452 10.1029/2007JB005154
- 453 Linker, M. F., & Dieterich, J. H. (1992). Effects of variable normal stress on rock  
 454 friction: Observations and constitutive equations. *J. Geophys. Res. Solid  
 455 Earth*, *97*(B4), 4923–4940. doi: 10.1029/92JB00017
- 456 Lognonne, P. (2005). Planetary seismology. *Annual Review of Earth and Planetary  
 457 Sciences*, *33*(1), 571–604. doi: 10.1146/annurev.earth.33.092203.122604
- 458 Lu, Z., Yi, H., & Wen, L. (2018). Loading-induced earth's stress change over  
 459 time. *Journal of Geophysical Research: Solid Earth*, *123*(5), 4285–4306. doi:  
 460 10.1029/2017JB015243
- 461 Luo, Y., & Liu, Z. (2019). Slow-slip recurrent pattern changes: Perturba-  
 462 tion responding and possible scenarios of precursor toward a megathrust  
 463 earthquake. *Geochemistry, Geophysics, Geosystems*, *20*(2), 852–871. doi:  
 464 10.1029/2018GC008021
- 465 Manga, M., Zhai, G., & Wang, C.-Y. (2019). Squeezing marsquakes out of  
 466 groundwater. *Geophysical Research Letters*, *46*(12), 6333–6340. Retrieved  
 467 from [https://agupubs.onlinelibrary.wiley.com/doi/abs/10.1029/  
 468 2019GL082892](https://agupubs.onlinelibrary.wiley.com/doi/abs/10.1029/2019GL082892) doi: 10.1029/2019GL082892
- 469 Milbert, D. (2018). *Solid*. <https://geodesyworld.github.io/SOFTS/solid.htm>.  
 470 (version update used: 2018-Jun-07)
- 471 Ross, Z. E., Trugman, D. T., Hauksson, E., & Shearer, P. M. (2019). Searching for  
 472 hidden earthquakes in southern california. *Science*, *364*(6442), 767–771. Re-  
 473 trieved from <https://science.sciencemag.org/content/364/6442/767> doi:  
 474 10.1126/science.aaw6888
- 475 Rubin, A. M., & Ampuero, J.-P. (2005). Earthquake nucleation on (aging) rate and  
 476 state faults. *Journal of Geophysical Research: Solid Earth*, *110*(B11). doi: 10  
 477 .1029/2005JB003686
- 478 Rubinstein, J. L., La Rocca, M., Vidale, J. E., Creager, K. C., & Wech, A. G.  
 479 (2008). Tidal modulation of nonvolcanic tremor. *Science*, *319*(5860), 186–  
 480 189. doi: 10.1126/science.1150558
- 481 Scholz, C. H., Tan, Y. J., & Albino, F. (2019). The mechanism of tidal triggering of

- 482 earthquakes at mid-ocean ridges. *Nature communications*, *10*(1), 2526. doi: 10  
 483 .1038/s41467-019-10605-2
- 484 Tanaka, S. (2012). Tidal triggering of earthquakes prior to the 2011 tohoku-oki  
 485 earthquake (mw 9.1). *Geophysical Research Letters*, *39*(7). doi: 10.1029/  
 486 2012GL051179
- 487 Tanaka, S., Ohtake, M., & Sato, H. (2002). Evidence for tidal triggering of earth-  
 488 quakes as revealed from statistical analysis of global data. *Journal of Geophys-  
 489 ical Research: Solid Earth*, *107*(B10). doi: 10.1029/2001JB001577
- 490 Thomas, A. M., Bürgmann, R., Shelly, D. R., Beeler, N. M., & Rudolph, M. L.  
 491 (2012). Tidal triggering of low frequency earthquakes near parkfield, california:  
 492 Implications for fault mechanics within the brittle-ductile transition. *Journal  
 493 of Geophysical Research: Solid Earth*, *117*(B5). doi: 10.1029/2011JB009036
- 494 Thomas, A. M., Nadeau, R. M., & Bürgmann, R. (2009). Tremor-tide correlations  
 495 and near-lithostatic pore pressure on the deep san andreas fault. *Nature*,  
 496 *462*(7276), 1048–1051. doi: 10.1038/nature08654
- 497 Tolstoy, M., Vernon, F. L., Orcutt, J. A., & Wyatt, F. K. (2002). Breathing of the  
 498 seafloor: Tidal correlations of seismicity at Axial volcano. *Geology*, *30*(6), 503-  
 499 506. doi: 10.1130/0091-7613(2002)030<0503:BOTSTC>2.0.CO;2
- 500 Ueda, T., & Kato, A. (2019). Seasonal variations in crustal seismicity in san-in dis-  
 501 trict, southwest japan. *Geophysical Research Letters*, *46*(6), 3172–3179. doi: 10  
 502 .1029/2018GL081789
- 503 Yabe, S., Tanaka, Y., Houston, H., & Ide, S. (2015). Tidal sensitivity of tectonic  
 504 tremors in nankai and cascadia subduction zones. *Journal of Geophysical Re-  
 505 search: Solid Earth*, *120*(11), 7587-7605. doi: 10.1002/2015JB012250